Phased Arrays—Part I: Theory and Architectures

Don Parker, *Life Fellow, IEEE,* and David C. Zimmermann, *Member, IEEE*

Invited Paper

***Abstract*—An overview of electronically scanned array technology with a brief introduction of the basic theory and array architectures are presented. Implementations, current state-of-the-art, and future trends are briefly reviewed in Part II of this paper.**

***Index Terms*—Active arrays, active element pattern, active reflection coefficient, array-element factor, electronically scanned arrays, hybrid arrays, passive arrays, phased arrays.**

I. Introduction

SINCE agile beams of electronically scanned arrays (ESAs) provide significant system advantages, phased-array technology is receiving considerable attention by the military and industry for airborne-, space-, surface-, and ground-based applications. Phased-array antennas first gained interest and development throughout the 1950s and 1960s [1]–[5], [36], [6]–[8]. There are two general types of phased arrays, i.e., passive and active. Passive arrays use a central transmitter and receiver, but have phase-shift capability at each radiating element or subarray. In active arrays, the high-power generation for transmit and low-noise amplification on receive are distributed, as is the phase control at each radiating element. Active arrays provide added system capability and reliability; but they did not receive extensive attention until the last 15 years because they were too complex and expensive. However, with the need to counter stealth technology, the advent of relatively low-cost GaAs monolithic microwave integrated circuits (MMICs), automated assembly of microwave components, and low-cost high-speed high-throughput digital-processor active arrays are becoming the preferred approach for many radar systems and communication systems requiring rapid scanning [9], [10].

Although the cost of active electronically scanned arrays (AESAs) has decreased by an order of magnitude in the last ten years and efforts are in progress to reduce them by another factor of 5–10, affordability is still a challenge. Space-based radar and communication applications also require additional significant reductions in array weight.

II. Array Electrical Architecture

Shown in Fig. 1 are two basic ESA architectures: the passive array and active array. Each has its unique properties, advantages, and shortcomings. Generally, in a passive array, there is no element amplitude control; only bilateral phase shifters are used at each element to provide the required phase shift for scanning, as illustrated in Fig. 1(a). The design challenge in a passive array is to minimize the losses in the feed network and the phase shifters in order to increase the system sensitivity and efficiency. This requirement often limits the type of RF feed network to waveguide and may increase the weight of an array appreciably. A passive array is generally the least expensive type of ESA because the number and cost of components is least. If very low sidelobe levels are required, a separate receive feed network with the appropriate amplitude weighting is used.

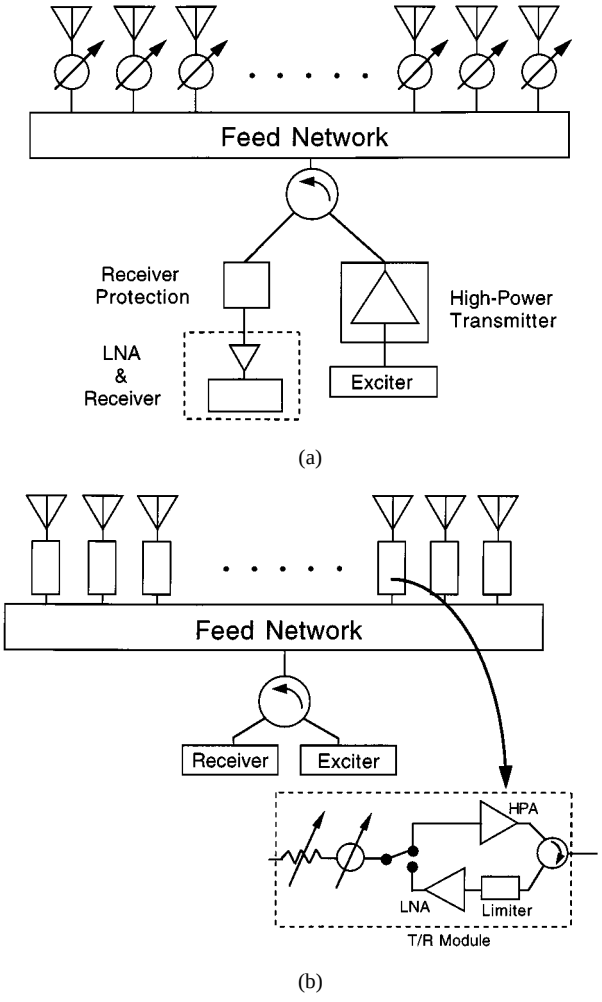

Fig. 1. Basic scanning array architectures. (a) Linear passive array with phase shifters for every element. (b) An active array with TRMs at every element.

Manuscript received August 15, 2001.

D. Parker, retired, was with Raytheon Electronic Systems, El Segundo, CA 90245 USA. He is now at 1728 Seven Oaks Lane, Ogden, UT 84403 USA (e-mail: dcjparker@earthlink.net).

D. C. Zimmermann is with Raytheon Electronic Systems, Dallas, TX 75266 USA (e-mail: d.zimmermann@ieee.org).

Publisher Item Identifier S 0018-9480(02)01989-0.

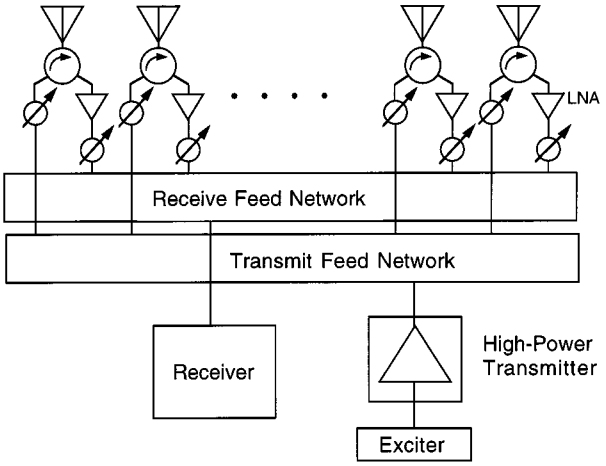

Fig. 2. Hybrid array architectures uses a central transmitter, distributed LNAs, and separate transmit and receive feed manifolds.

In an active array, a transmit/receive module (TRM) is used at each element to provide amplitude and phase control. The central transmitter used in a conventional passive array is replaced by the distributed power amplifiers in each TRM, as illustrated in the simplified block diagram of a TRM shown in the inset of Fig. 1(b). The reader is referred to a companion paper on TRMs in this TRANSACTIONS for a discussion of the design, properties, and performance of TRMs [11]. The principle advantage of an active array is that the system sensitivity is increased because the system noise figure is set and the RF power is generated at the aperture. A second advantage is that the TRMs provide complete flexibility in amplitude and phase control for both transmit and receive. A third advantage of an active array is that the feed networks need not be optimized for lowest loss; thereby allowing design flexibility and the ability to minimize size (volume) and weight. Of course, these performance improvements come with increased array complexity and cost.

A hybrid phased-array combines some features of passive and active arrays, as illustrated in Fig. 2. A central transmitter feeds the array as in a conventional passive phased array, but a low-noise amplifier (LNA) is placed at each element in front of the phase shifters to improve the overall system noise figure. A limiter may be required in front of the LNA for protection, as in an active array. A separate receive feed network is used and optimized for low sidelobes. It is also possible in a hybrid array to distribute medium power transmitters, e.g., in each column of the array, to provide increased system reliability.

For very large arrays and systems with very wide instantaneous bandwidths, array architecture with true time delay (TTD) is required to prevent signal distortion and beam squinting. In this type of array, the length of the transmission line feeding each element provides the differential phase shift. To scan the beam, however, the effective line length of the feed lines to each element must be changed accordingly. Several methods for changing line lengths have been suggested including switchable fiber-optic delay lines, but the technology is immature [10].

III. Array Physical Configurations

Physical realization of active arrays has followed three basic structures referred to as "brick," "tile," and "tray"in accordance with the physical layout of the TRMs and corresponding subarrays comprised of cold plate, signal and power distribution, and feed networks. In brick-style arrays, the TRMs are rectangular in shape like a brick and are mounted on both sides of cold plates along with energy storage capacitors, signal and power distribution circuits, and RF manifolds to form linear subarrays, as illustrated in Fig. 3(a) [12]. A set of these subarrays are stacked together to form a planar array, as shown in Fig. 3(b). The radiators may be attached to each subarray or they may be in a separate aperture plate that the subarrays plug in to. The tray architecture is effectively the same as the brick architecture, except that each subarray is self-contained with its own power supply and beamsteering controller. Tray architecture was used in the ground-based radar for THAAD [9].

In tile array architecture, the TRMs are shaped like rectangular tiles and are mounted on a cold plate that is parallel to the aperture [13]. The energy storage, the signal and power distribution circuits, and the RF manifolds are mounted behind the TRMs parallel to the aperture in a configuration like the layers of a cake. Tile architectures have led to significant reductions in array weight, but have required improved cold plate designs and new novel RF and dc blind interconnections. Fig. 4 presents a photograph of two ladies holding a tile array suitable for fighter fire control radar. It is unlikely they could hold a brick array designed for the same application. Also shown in Fig. 4 is a photograph of a three-layer tile TRM. Techniques for arraying tile subarrays are being investigated for applications requiring very large lightweight apertures.

IV. Array Scanning Theory

The radiation patterns of linear and planar-phased arrays are a function of each element's physical structure, its excitation, and the array lattice. Usually, similar radiators are arranged in a linear, rectangular, or triangular lattice with periodic spacing between radiating elements. Arrays with the radiators arranged in concentric circles have certain advantages such as lower first sidelobes. When identical radiators are used in a large rectangular array, the radiation pattern is the product of two factors. One, i.e., the element factor, is a function of the radiator physical realization; the other, i.e., the array factor, is a function of the array geometry, and the element excitations. For the purposes of this paper, we will assume that the array factor and element factor are separable and the radiation pattern is the product of the element and array factors. Therefore, we will use only the array factor in describing the array scanning characteristics. The following analysis follows that of [2], [5], [36], [14].

V. Linear Arrays

Consider an array of identical radiators, $2N + 1$ in number, equally spaced by a distance d along the z-axis, as shown in Fig. 5. All elements have similar current distributions that differ only in magnitude and phase. I_n is the magnitude of the current on the nth element. For this linear array, the array factor $F_a(\theta, \phi)$ is proportional to the radiated field at a point in space

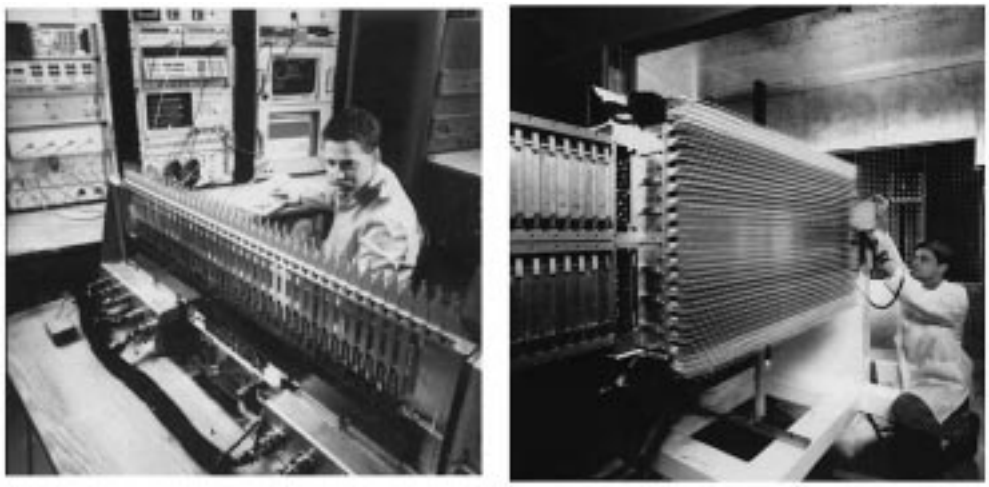

(a) (b)

Fig. 3. "Brick" active array. (a) TRMs, radiators, RF manifolds, and signal and power distribution are mounted on linear subarrays. (b) Several subarrays are stacked together to form a planer array.

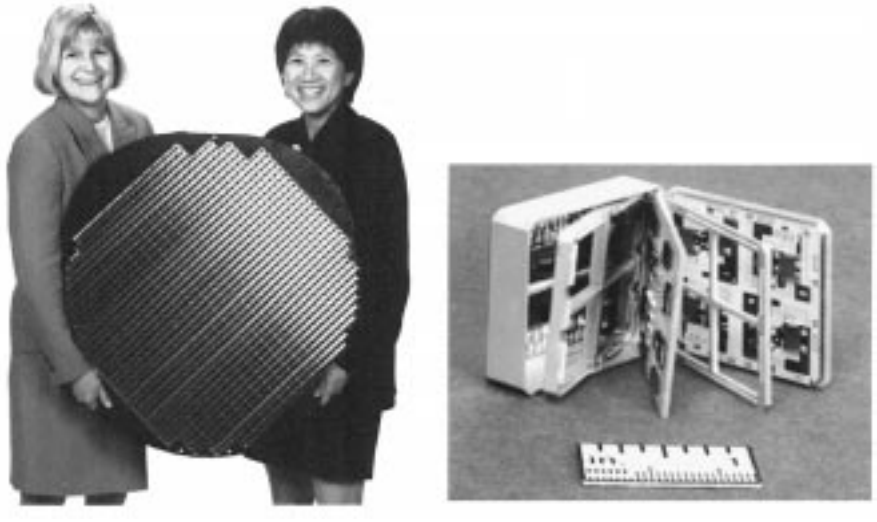

(a) (b)

Fig. 4. Lightweight "tile" array for airborne applications. The three-layer tile TRMs, cold plate, RF, and dc distribution networks are mounted on the array back parallel to the aperture like layers of a cake.

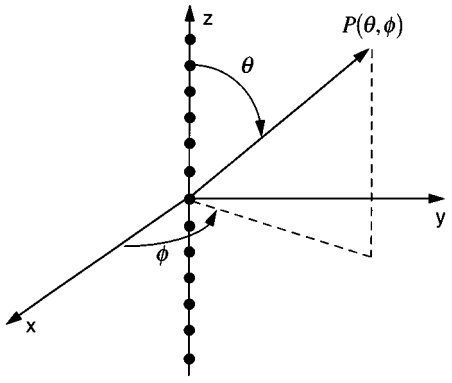

Fig. 5. Linear array with the elements equally spaced along the z-axis. θ and ϕ are angles from the origin (zero element) to a point P in space.

described by (θ, ϕ)

$$F_a(\theta, \phi) = \sum_{n=-N}^{n=N} \frac{I_n}{I_o} e^{jnkd\cos\theta} \tag{1}$$

where $k = 2\pi/\lambda$ and λ is the wavelength. For a linear array, $F_a(\theta, \phi)$ is rotationally symmetric about the z-axis (independent of ϕ).

If the currents are equal and in phase, (1) reduces to

$$F_a(\theta, \phi) = \sum_{n=-N}^{n=N} e^{jnkd\cos\theta}. \tag{2}$$

The array factor is equal to a sum of phasors of unity magnitude with progressive multiples of the basic angle ψ

$$\psi = \frac{2\pi d}{\lambda}\cos\theta. \tag{3}$$

We are mostly interested in those cases where the length of the array L is very large compared to a wavelength $(L \gg \lambda)$ and the element spacing d is less than a wavelength, i.e., $d < \lambda$. In these instances, the array pattern gives a narrow beam broadside to the array axis ($\theta = \pi/2$) with several sidelobes. An example is plotted in Fig. 6 for a 15-element array.

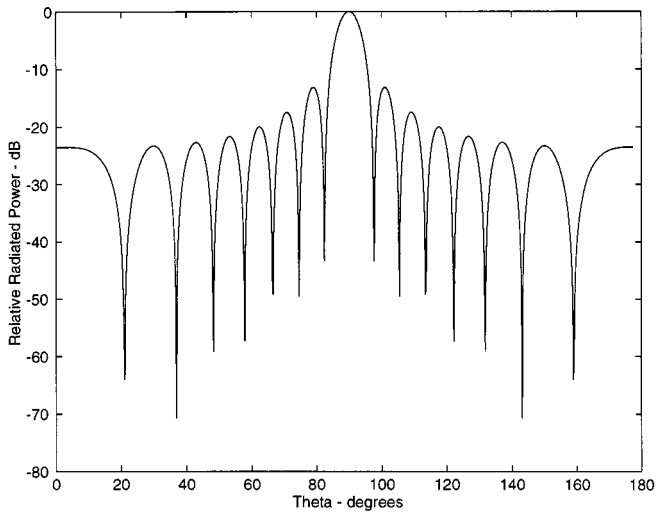

Fig. 6. Radiation (power) pattern of 15-element linear array relative to the peak of the main beam. Elements are equally spaced a distance of a half-wavelength.

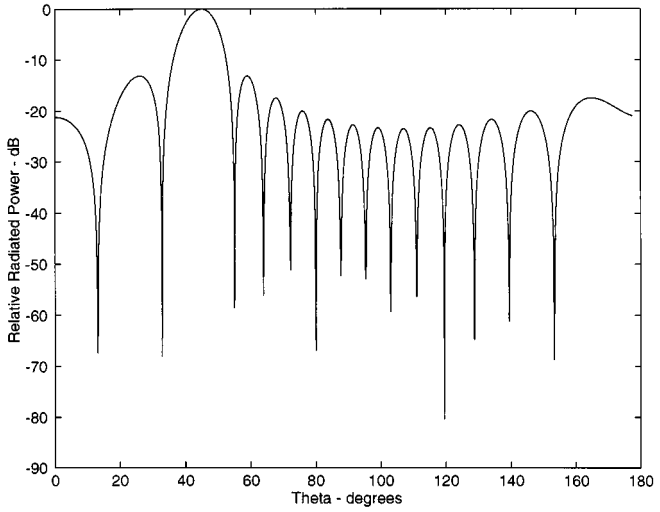

Fig. 7. Radiation pattern of a 15-element equally spaced linear array scanned 45° off broadside. Element spacing is a half-wavelength.

The first sidelobe is 13.5 dB below the peak of the main beam and the peak of each successive sidelobe is even lower as its distance from the main beam increases.

Tapering the magnitude of the currents across the array can decrease the sidelobes. The central element is fed with the largest current and the magnitudes of the currents in the other elements are symmetrically tapered. As a result, the sidelobes are reduced, but the width of the main beam (beamwidth) is increased. Several synthesis techniques have been developed to realize tapered apertures [15] (see also [14, Ch. 5] and [16, Ch. 3]).

VI. Directivity of Linear Arrays

A measure of an antenna is its gain or directivity over that of an isotropic radiator. The gain is equal to the directivity if there are no ohmic or mismatch loss. Antenna directivity in the direction of maximum radiation θ_o is defined as the ratio of maximum power radiated per unit solid angle divided by the average power radiated (total power radiated divided by 4π) or

$$D = \frac{|E(\theta_o)|^2}{|E(\theta)|^2_{\text{average}}} \tag{4}$$

where $|E(\theta)|^2_{\text{average}}$ is equal to the average of $|E(\theta)|^2$ over 4π sr and $E(\theta)$ is the radiated electric field that includes the effects of the element pattern and the array pattern [17], [18]. The directivity of a uniformly weighted linear array of N isotropic radiators spaced $\lambda/2$ apart is equal to N independent of the main beam scan angle θ_o. For nonuniformly weighted linear arrays, the directivity is given by

$$D = \frac{2d}{\lambda} D_o \tag{5}$$

where D_o is given by the relation

$$D_o = \frac{\left[\sum_{n=-N}^{n=N} I_n\right]^2}{\sum_{n=-N}^{n=N} I_n^2}. \tag{6}$$

There is no simple formula for determining the directivity of an array of nonisotropic elements, as one must know the current distributions in each radiating element. However, as will be shown later, there is a very useful equation for determining the realized gain of an array in terms of the realized gain of a radiating element embedded in a large uniformly weighted array.

VII. Scanned Linear Array

To scan the linear array in Fig. 5, assume that the element currents all have equal amplitudes and a uniform progressive phase α_z as follows:

$$I_n = I_o e^{-jn\alpha_z}. \tag{7}$$

Equation (2) then becomes

$$F_a(\theta, \phi) = \sum_{n=-N}^{n=N} e^{jn(kd\cos\theta - \alpha_z)}. \tag{8}$$

Equation (8) differs from (2) only in an angular shift in the origin. Thus, the uniform progressive phase factor α_z changes the peak beam position from broadside to another angle in space θ_o given by

$$kd\cos\theta_o = \alpha_z \text{ or } \theta_o = \arccos\left[\frac{\alpha_z}{2\pi}\frac{\lambda}{d}\right]. \tag{9}$$

When α_z is changed electronically, the array is called an ESA. Fig. 7 shows the beam of the equally spaced 15-element linear array scanned 45° off broadside.

VIII. Grating Lobes

If the element spacing d is too large compared to a wavelength, a second main beam called a grating lobe will appear in the radiation pattern. From (7), it is evident that this will happen at an angle θ', where

$$kd\cos\theta' - \alpha_z = \pm 2\pi \text{ or } \cos\theta' = \cos\theta_o \pm \frac{\lambda}{d}. \tag{10}$$

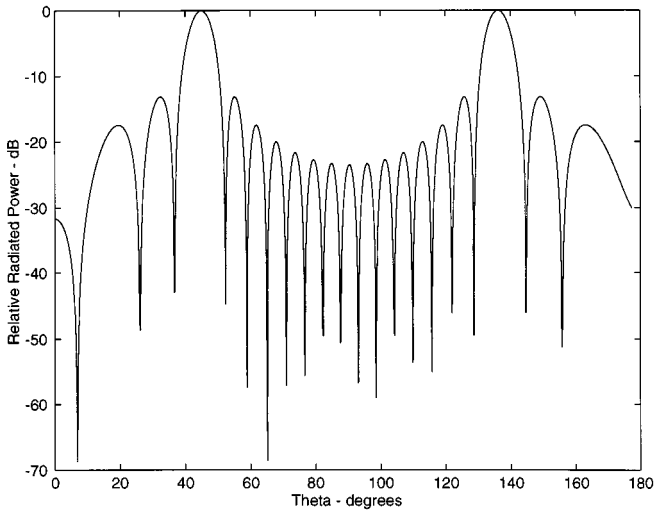

Fig. 8. Radiation pattern of a 15-element array with equally spaced elements 0.7 wavelengths apart scanned to 45°. A grating lobe appears at 135°.

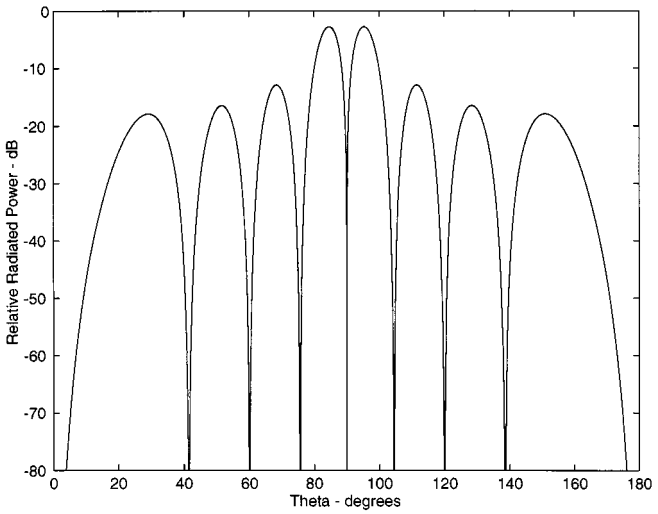

Fig. 9. Difference pattern of a 16-element equally spaced array realized by exciting half the array 180° out-of-phase with the other half.

To prevent a second main beam, the spacing d must be chosen to satisfy the following condition:

$$\frac{d}{\lambda} < \frac{1}{1+|\cos\theta_o|}. \tag{11}$$

Thus, the elements must be spaced one half-wavelength apart to prevent a second main beam when scanning close to endfire ($\theta_o = 0$ or π).

Fig. 8 shows a grating lobe appearing in real space when the beam of a 15-element array with elements equally spaced at 0.7 of a wavelength is scanned off broadside.

IX. Bragg Lobes

For military applications where stealth is a requirement, phased arrays are preferred because they can be designed with low self-signature. The element spacing is small to prevent Bragg lobes in the direction of the threat radar [10, ch. 39]. Bragg lobes are retro-directive reflections that may be received by illuminating radar at an angle off broadside if the radiator spacing is larger than a half-wavelength. Specifically, when adjacent radiators in an array are illuminated by a threat radar, a Bragg lobe will be produced if the waves reflected in the radar's direction by the two radiators are in phase by a whole multiple of the incident radiation's wavelength, i.e., $n\lambda_r$. The total round trip difference in distance between the radiators is equal to $2d\sin\theta_r$, where d is the spacing between radiators and θ_r is the angle of the threat radar. Thus, the relationship between radiator spacing and the Bragg-lobe direction is

$$d = \frac{n\lambda_r}{2\sin\theta_r}. \tag{12}$$

To minimize the antenna's radar cross section, the first Bragg lobe ($n = 1$) must be 90° off broadside ($\sin\theta_r = 1$) or $d \leq \lambda_r/2$ for stealth.

X. Array Difference Patterns

If the number of elements in an equally spaced linear array is even, it is possible to realize a symmetrical difference pattern consisting of two main beams, as illustrated in Fig. 9. Difference patterns are realized by exciting the two halves of the array out-of-phase with each other.

In Fig. 9, the currents in each element are equal in magnitude, but out-of-phase on the two halves of the array. A uniform progressive phase given to each current distribution with the two halves of the array still excited out-of-phase with each other will produce a scanned difference pattern.

Sum patterns like that shown in Fig. 6 and difference patterns such as shown in Fig. 9 are used in radar applications to acquire and track targets. The sum pattern of a single beam is useful for acquiring a target, but the beam is too broad to precisely determine its location. The target is illuminated with the sum pattern and when the target is close enough, the difference pattern is used on receive with the beam shifted to keep the target between its two main beams. Except when the target is exactly in the null between the two principal lobes of the difference pattern, a return signal is detected in the radar receiver. This signal is proportional to the slope of the pattern in the center null between the principal lobes and, therefore, is very sensitive to the position of the beam. The angular position of the target can be determined accurately.

XI. Planar Arrays

Planar arrays are of considerable importance in radar and communication applications. The basic principles of beam forming and scanning discussed above for linear arrays can be readily extended to planar arrays. Consider a rectangular planar array with the elements arranged in a rectangular grid, as shown in Fig. 10.

The spacing between elements in the x-direction is d_x and the element spacing in the y-direction is d_y. If there are $2N_x + 1$ rows of elements parallel to the y-axis and each row contains $2N_y + 1$ elements, the array factor can be written as

$$F_a(\theta, \phi) = \sum_{m=-N_x}^{m=N_x} \sum_{n=-N_y}^{n=N_y} \left(\frac{I_{mn}}{I_{oo}}\right) e^{jk\sin\theta(md_x\cos\phi + nd_y\sin\phi)} \tag{13}$$

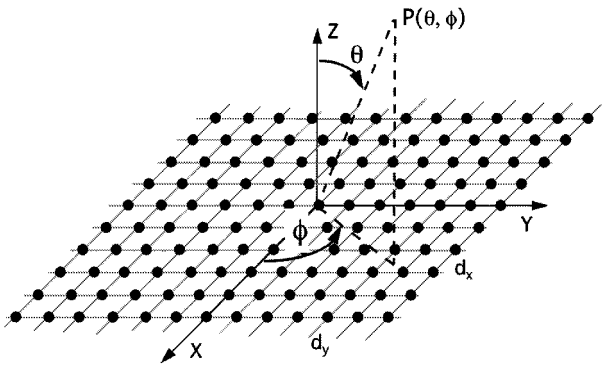

Fig. 10. Planar array of elements on a rectangular lattice with element spacing d_x in the x-direction and d_y in the y-direction.

where I_{mn} is the current distribution in the mnth element. If each row has the same current distribution even though the current levels are different, i.e., $I_{mn}/I_{mo} = I_{on}/I_{oo}$, then the current distribution is said to be separable and the array factor can be expressed in the form

$$F_a(\theta, \phi) = F_x(\theta, \phi)F_y(\theta, \phi) \tag{14}$$

where

$$F_x(\theta, \phi) = \sum_{-N_x}^{N_x} I_m e^{jmkd_x \sin\theta\cos\phi} \tag{15}$$

$$F_y(\theta, \phi) = \sum_{-N_x}^{N_x} I_n e^{jnkd_y \sin\theta\sin\phi} \tag{16}$$

and

$$I_m = \frac{I_{mo}}{I_{oo}} \quad I_n = \frac{I_{on}}{I_{00}} \tag{17}$$

are the normalized current distributions in a row of elements parallel to the x-axis and the y-axis, respectively. The array factors in (15) and (16) can be recognized as representing linear arrays parallel to the x- and y-axes. Thus, under the stated restriction that the aperture distribution is separable, the array factor for a rectangular grid array with a rectangular boundary is the product of the array factors for two linear arrays, one laid out along the x-axis and the other laid out along the y-axis.

If the current distributions I_m and I_n have uniform phase progression $\alpha_x = kd_x \sin\theta_o \cos\phi_o$ in the x-direction and $\alpha_y = kd_y \sin\theta_o \sin\phi_o$ in the y-direction, the array factor is now given by

$$F_a(\theta, \phi) = \left[\sum_{-N_x}^{N_x} I_m e^{jm(kd_x \sin\theta\cos\phi - \alpha_x)}\right] \times \left[\sum_{-N_y}^{N_y} I_n e^{jn(kd_y \sin\theta\sin\phi - \alpha_y)}\right] \tag{18}$$

and the current amplitudes I_m and I_n are now pure real. By selecting the element pattern to give negligible radiation in the half-space $z < 0$, through use of a ground plane, for example, a single main pencil beam is left pointing in the unique direction (θ_o, ϕ_o) for $z > 0$. Fig. 11 shows a three-dimensional plot of the radiation pattern of a rectangular array with the main beam pointing in the direction $\theta_o = 30°$ and $\phi_o = 90°$.

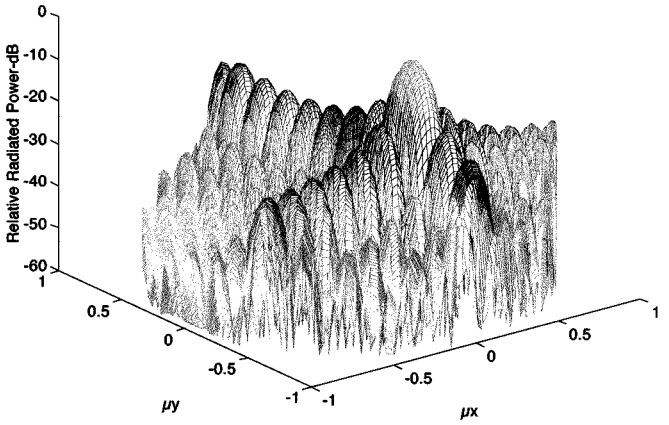

Fig. 11. Radiation pattern of 15 × 11 element planar array scanned 30° along the y-axis. $u_x = \sin(\theta)\cos(\phi)$ and $u_y = \sin(\theta)\cos(\phi)$, d_x and d_y equal one half-wavelength.

It is clear from Fig. 11 that sidelobes surround the main beam and all of the off-axis sidelobes are lower than the sidelobes along the principal x-axis and y-axis. The low sidelobe levels in the inter-cardinal planes, characteristic of separable distributions, are achieved at the price of beam broadening. To achieve a ϕ-symmetric pattern, consisting of a pencil beam and a family of concentric rings of a common height sidelobes, one must use a nonseparable aperture distribution. A common configuration is a planar aperture with a circular boundary with the elements equally spaced on concentric circles [19].

XII. Statistical Theory of Arrays

The elements in all arrays have random errors in amplitude and phase. Active arrays in particular experience random errors because of process variations used in the manufacture of TRMs and their internal MMIC circuits. Since typically there are more than 1000 elements in an array, it is beneficial to specify TRMs and components for TRMs statistically on a lot basis. Significant increases in yield and reduced costs have been realized with little degradation in array performance.

The effects of the remaining amplitude and phase errors are decreased peak of the antenna main beam, beam-pointing error, and increased sidelobe level. Fortunately, adjusting phase-shifter control settings within limits can minimize the effects of amplitude and phase errors.

It is convenient to characterize the effects of the residual errors on the array factor statistically, and studies have been extensively documented in the literature [4], [6], [20]–[29]. In these treatments, array average pattern characteristics are determined. The results do not pertain to any one antenna, but describe the observed results averaged over a large number of arrays that have the same statistical phase and amplitude errors. Here, we follow the analysis of [4] and [23].

An array is assumed to have an amplitude error δ_n and a phase error ϕ_n at the nth element. The meaning of the amplitude error δ_n is that the excitation at the nth element has amplitude $(1 + \delta_n)I_n$, where I_n is the correct amplitude. The meaning of the phase error ϕ_n is that the correct phase to steer a beam to the chosen angle is not the correct excitation, but is $\exp(j\phi_n)$ times the correct excitation.

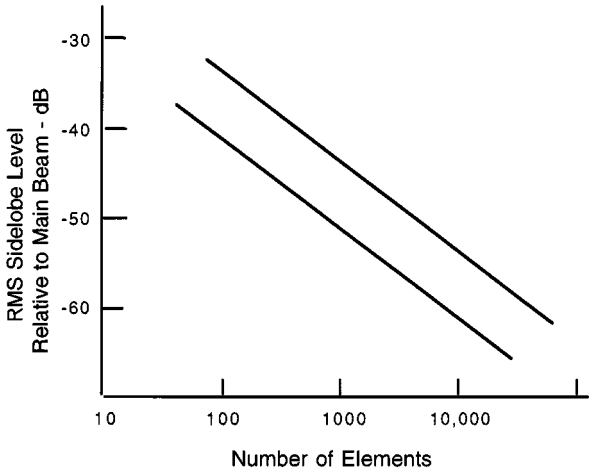

Fig. 12. Plot of residual sidelobe error. Top curve is for rms phase error of 10° and amplitude error of 1 dB. Bottom curve is rms phase error of 3.5° and amplitude error of 0.5 dB. Most active arrays are within these limits.

Only random errors are considered and it is assumed that the phase error is described by a Gaussian probability density function with zero mean and variance $\overline{\phi^2}$. The amplitude error δ_n has zero mean and variance $\overline{\delta^2}$. Under these conditions, Skolnik derived an expression for a normalized array factor that is equal to a normalized ideal pattern plus a term for a normalized sidelobe level $\overline{\sigma^2}$, sometimes referred to as the residual sidelobe level.

For an array of N isotropic elements, the residual sidelobe level is given by

$$\overline{\sigma^2} = \frac{\overline{\phi^2} + \overline{\delta^2}}{N\eta_T} \tag{19}$$

where η_T is an array taper efficiency equal to one for uniform aperture distributions and less than one for tapered apertures. Thus, for any given array variance, increasing the size of the array lowers the actual value $\overline{\sigma^2}$ of the residual sidelobes.

Fig. 12 is a plot of the residual sidelobe level as a function of the number of array elements without aperture taper. Two different levels of residual sidelobe errors relative to the main beam are shown. The top curve is for rms phase error of 10° and amplitude error of 1 dB. The bottom curve is for rms phase error of 3.5° and amplitude error of 0.5 dB. Today, the errors for most active arrays fall within these limits. Tapering the array aperture distribution increases the residual sidelobe level for given array variances.

The reduction in array directivity due to residual errors is given approximately by [23] as

$$\frac{D}{D_{ef}} = \frac{1}{1 + \overline{\delta^2} + \overline{\phi^2}} \tag{20}$$

where D is the directivity of the array with errors and D_{ef} is the directivity of the error free array. The reduction in directivity is only a function of error variance and not array size.

Steinberg [24] has shown that the variance of beam pointing deviation $\overline{\Delta^2}$ is given by

$$\overline{\Delta^2} = \frac{12}{N^3}\overline{\phi^2}. \tag{21}$$

XIII. Self-Impedance and Mutual Coupling

Radiation from antenna elements in an array is different than when isolated because of mutual coupling between elements. In the previous sections, we assumed that all the current distributions on the elements were identical and differed only in magnitude and phase from element to element. Further, it was assumed that the current distributions did not change as the array is scanned. For finite arrays, these assumptions are not valid because mutual coupling among the elements alters the current distributions. The center elements experience a different environment than the edge elements, and, therefore, have different current distributions that vary as a function of frequency and scan angle. Under these conditions, one cannot remove the element factor and consider only the array factor in determining the antenna radiation pattern characteristics. The procedure for determining the current distribution is very complex and usually requires solving a multiplicity of simultaneous integral or integrodifferential equations. These equations have been solved exactly only for certain idealized cases.

For large arrays where the total number of elements is much greater than the number of edge elements, it is reasonable to assume an infinite array to determine an array-element factor that accounts for the effects of mutual coupling. In an infinite array, every element sees an identical environment. Except for their phase, the current distributions on every element are the same and the array pattern is equal to the product of an array-element factor and an array factor, as discussed previously. However, it is more convenient to define an array factor for the radiated power rather than the radiated electric field. In defining this factor, it is assumed that the elements in the array are fed with constant-incident-power sources, as opposed to constant current or voltage sources. Actually, this assumption closely corresponds to most arrays at microwave frequencies.

We define the array-element factor $g_r(\theta, \phi)$ as the radiated power pattern obtained when one element is fed with a constant-incident-power source and all other elements are terminated with generator impedance matched to the transmission lines feeding the elements [6]. This array-element factor, also referred to as the imbedded-element pattern, contains all the effects of mutual coupling on the pattern over scan angles.

In a large array, we assume all of the elements have identical patterns and are excited with equal amplitude. The principle of superposition may then be combined with a consideration of the power available from the generators feeding the elements to yield the relation

$$G_r(\theta, \phi) = N g_r(\theta, \phi) \tag{22}$$

where $G_r(\theta, \phi)$ is the antenna gain realized in the direction (θ, ϕ) when the elements are excited to add in phase in that direction, $g_r(\theta, \phi)$ is the gain realized in the same direction when only one element is excited, and N is the number of elements.

Because of losses and impedance mismatches, the realized antenna gain is less than the directive gain of the antenna without these effects. If we assume that there are no dissipation losses in the antenna and feed lines and consider only the mismatch

losses, the ratio of the realized antenna gain $G_r(\theta, \phi)$ to directive gain $G_d(\theta, \phi)$ is given by

$$G_r(\theta, \phi)/G_d(\theta, \phi) = 1 - \left|\Gamma(\theta, \phi)\right|^2 \tag{23}$$

where $\Gamma(\theta, \phi)$ is the active reflection coefficient when all of the elements are driven by constant power sources with the appropriate phases to scan to (θ, ϕ). Thus, the effects of mutual coupling can be expressed in the form of an equivalent active reflection coefficient that is approximately the same for all elements in a large array.

For apertures large compared to a wavelength, the peak directive gain of a uniformly excited planar array with no grating lobes is related to the area of the array aperture

$$G_d(\theta, \phi) = (4\pi NA/\lambda^2)\cos(\theta) \tag{24}$$

where A is the area associated with each element (equal to $d_x d_y$ for a rectangular array) and (θ, ϕ) is the direction in which all the elements add in phase [2], [4]. Combining (22)–(24), we obtain an expression for the array-element factor

$$g_r(\theta, \phi) = (4\pi d_x d_y/\lambda^2)\cos(\theta)\left[1 - \left|\Gamma(\theta, \phi)\right|^2\right]. \tag{25}$$

Equation (25) is a very useful relationship because it relates two different conditions of operation of an array. The array-element factor is obtained by exciting only one element at a time with all other elements terminated in their generator impedance. The active reflection coefficient is determined when all of the elements in the array are excited with the proper phases to point the beam in the direction (θ, ϕ) and is a measure of the power reflected by an element.

The mutual coupling between array elements and its effect on the antenna gain and active reflection coefficient are embedded in the array-element factor. An approximation of this factor can be measured by exciting a center element of a smaller array with a sufficiently large number of elements, or it can be determined by measurement of $\Gamma(\theta, \phi)$ over restricted scan angles using waveguide simulators, or $\Gamma(\theta, \phi)$ can be calculated using computer models of waveguide simulators.

XIV. Array Scanning Simulation

The discussion in this section reflects a personal communication from R. L. Eisenhart and is based on his work [31]. Waveguide simulators were introduced almost 40 years ago to determine the active element pattern (AEP) (equivalent to the array-element factor) of a radiator imbedded in a large array. They have been effective in verifying the design of large arrays without the expense of building and testing full-size arrays. Recently, commercial computer programs became available that can model the electromagnetic-field distributions of three-dimensional circuits. Eisenhart has successfully applied these computer programs to calculate the active reflection coefficient of large arrays as a function of scanning angle [30]–[32]. Computer modeling avoids the hardware complexity and associated scan limitations of conventional waveguide simulators. Another advantage of these programs is the ability to use magnetic walls as well as electric (metal) walls; thereby allow modeling of circuits that could never be measured with real hardware.

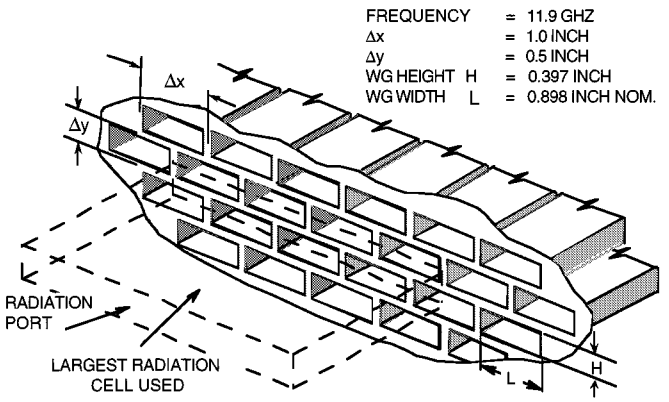

Fig. 13. Active reflection coefficient was computed for a triangular array of open-ended waveguides to demonstrate the power of computer simulation. Multicell radiation waveguide allows simultaneous simulation of many different scan angles.

Waveguide simulation (real and computer models) is based upon the principle of imaging all of the elements of an infinite array into a single waveguide "radiation" cell. The simulator models uniformly excited infinite arrays (approximates large finite arrays), and the imaging accounts for all mutual coupling effects between elements. However, for a given specific array lattice, only certain scan angle/frequency conditions can be simulated. For additional scan angles, one must use multicell simulators with complex higher order modes. Hardware testing requires the construction of special higher order mode transitions for each of the scan angles desired and one mode is tested at a time. On the other hand, computer simulations allow simultaneous multiple scan values to be evaluated because they can deal independently with the higher modes in a single multicell model. By mixing various combinations of electric and magnetic walls in a multicell simulator, many scan conditions are possible including broadside, H-plane, E-plane, and off-principal planes.

To determine the active reflection coefficient $\Gamma(\theta, \phi)$ and the AEP by simulation, a radiation cell is defined based upon the array lattice dimensions. The array element is first matched ($\Gamma = 0$) for broadside scan. The active reflection coefficient for scan angles off broadside is then calculated by using higher order modes in multicells and various size radiation cells.

For example, Eisenhart computed the AEP for the triangular array of open-ended waveguide radiators shown in Fig. 13. The dashed lines in front of the array face outlines the radiation cell or simulating waveguide that contains the effect of all of the array element images. The largest cell he used is shown and it provided eight scan points in the H-plane. Smaller width radiating waveguide cells were also used to provide additional scan angles. He simulated three different arrays with waveguide widths W equal to 0.858, 0.898, and 0.938 in. All other dimensions were fixed.

The reflection coefficient data from each of four multicell simulations was used to calculate the AEP for each of the three different waveguide widths. The results are shown in Fig. 14. Note that less than $\pm 5\%$ change in waveguide width results in significant performance changes in the AEP.

The three marks at the bottom of the graph in Fig. 14 are the predicted scan angles for high reflection or blindzone (BZ) cen-

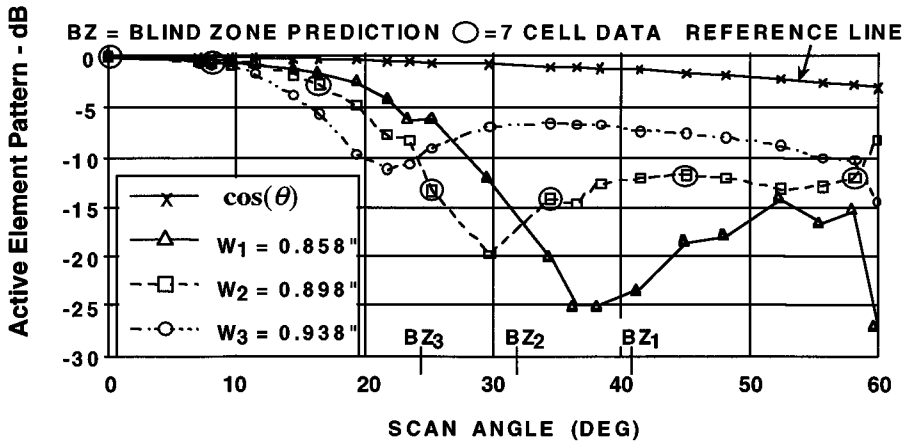

Fig. 14. Simulated scan performance for the waveguide triangular array in Fig. 13. Note that the data from different radiation cell configurations complement each other to form a near continuous scan prediction. Performance is shown to be very sensitive to element dimensions and correlates well with theory based on a two-mode approximation.

ters for the three configurations, as determined by an approximate theory [33]. A BZ occurs in the AEP when the scan phasing is such that the mutual coupling constructively provides a high reflection at the element being analyzed [34], [35].

Eisenhart's simulation results agree closely with the theoretical predictions. His are likely to be more accurate because all higher order waveguide modes are included in the determination of $\Gamma(\theta, \phi)$ rather than just the two modes in the approximate theory. The reference line curve indicates the rolloff of the pattern due to the reduction in array projected area with increasing scan angle.

The performance characteristics of scanned arrays are easily determined using computer simulations, allowing for fast and inexpensive design. Particularly significant is the ability to model complex three-dimensional radiating elements such as flared-notch radiators that are not tractable with other theoretical approaches.

XV. Summary

The system advantages of phased arrays has been known, studied, and developed for the past 60 years. Initial implementations were passive because the technology of active arrays was immature and too costly. With the advent of MMIC technology, automated assembly of microwave components, and high-speed digital processors, active arrays are becoming the preferred approach for both radar and communication systems in airborne, ground, and space application. Commercial simulation tools are facilitating the design of array apertures and radiators, as well as the components used in phased arrays.

Acknowledgment

The authors acknowledge the help of T. C. Cisco, Raytheon Electronic Systems, El Segundo, CA, and H. Shyu, Raytheon Electronic Systems, El Segundo, CA, for providing information and photographs for this paper. We also wish to thank Dr. R. L. Eisenhart, Eisenhart and Associates, Woodland Hills, CA, for providing information in Section XIV to determine the AEP of an array with mutual coupling.

References

[1] R. C. Hansen, Ed., *Microwave Scanning Antenna, Volume I Apertures*. New York: Academic, 1964.
[2] ——, *Microwave Scanning Antenna, Volume II Array Theory and Practice*. New York: Academic, 1966.
[3] R. C. Hansen, Ed., *Microwave Scanning Antenna, Volume III Array Systems*. New York: Academic, 1966.
[4] J. L. Allen, "The theory of array antennas," MIT Lincoln Lab., Lexington, MA, Tech. Rep. 323, 1963.
[5] R. S. Elliott, "Beamwidth and directivity of large scanning arrays," *Microwave J.*, pt. 1, vol. 6, pp. 53–60, Dec. 1963.
[6] A. A. Oliner and G. H. Knittel, *Phased-Array Antennas*. Norwood, MA: Artech House, 1972.
[7] R. C. Hansen, *Significant Phased Array Papers*. Norwood, MA: Artech House, 1973.
[8] E. Brookner, *Practical Phased-Array Antenna Systems*. Norwood, MA: Artech House, 1991.
[9] *IEEE Int. Phased-Array Syst. Technol. Symp. Dig.*, Boston, MA, Oct. 15–18, 1996.
[10] G. W. Stimson, *Introduction to Airborne Radar*, 2nd ed. Mendham, NJ: Science, 1998, ch. 37–39.
[11] B. Kopp, M. Borkowski, and G. Jerinic, "Transmit/receive modules," *IEEE Trans. Microwave Theory Tech.*, vol. 50, pp. 827–834, Mar. 2002.
[12] S. Panaretos, C. Shoda, R. Relatores, J. Gordon, P. Curtis, and D. Parker, "A broadband, low-sidelobe, dynamic weighting three-channel receive, X-band active array," in *IEEE MTT-S Int. Microwave Symp. Dig.*, vol. III, San Francisco, CA, June 1996, pp. 1573–1576.
[13] R. Sturdivant, C. Ly, J. Benson, and M. Hauhe, "Design and performance of a high density 3D microwave module," in *IEEE MTT-S Int. Microwave Symp. Dig.*, vol. 2, Denver, CO, June 1997, pp. 501–504.
[14] R. S. Elliott, *Antenna Theory and Design*. Englewood Cliffs, NJ: Prentice-Hall, 1981.
[15] E. T. Bayliss, "Design of monopulse antenna difference patterns with low side-lobes," *Bell Syst. Tech. J.*, vol. 47, pp. 623–650, May–June 1968.
[16] R. J. Mailloux, *Phased Array Antenna Handbook*. Norwood, MA: Artech House, 1994.
[17] E. Brookner, "Antenna array fundamentals part I," in *Practical Phased Array Antenna Systems*. Norwood, MA: Artech House, 1991, ch. 2.
[18] C. T. Tai, "The nominal directivity of uniformly spaced arrays of dipoles," *Microwave J.*, vol. 7, pp. 51–55, Sept. 1964.
[19] J. Colin, "Phased array radars in France: Present and future," in *IEEE Int. Phased Array Syst. Technol. Symp. Dig.*, Oct. 1996, pp. 458–459.
[20] J. Ruze, "Physical limitations on antenna," Res. Lab. Electron., Massachusetts Inst. Technol., Cambridge, MA, Oct. 1952.
[21] ——, "The effect of aperture errors on the antenna radiation pattern," *Nuovo Cimento (Suppl.)*, vol. 9, no. 3, pp. 364–380, 1992.
[22] R. E. Elliott, "Mechanical and electrical tolerances for two-dimensional scanning antenna arrays," *IEEE Trans. Antennas Propagat.*, vol. 6, pp. 114–120, 1958.
[23] M. I. Skolnik, "Non-uniform arrays," in *Antenna Theory*, R. E. Collin and F. J. Zucker, Eds. New York: McGraw-Hill, 1969, ch. 6, pp. 227–234.

[24] B. D. Steinberg, *Principles of Aperture and Array Systems Design*. New York: Wiley, 1976.
[25] H. J. Moody, "A survey of array theory and techniques," RCA Victor, Res. Labs., Montreal, QC, Canada, RCA Victor Rep. 6501.3, Nov. 1963.
[26] J. K. Hsiao, "Array sidelobes, error tolerance, gain and beamwidth," Naval Res. Lab., Washington, DC, NRL Rep. 8841, Sept. 28, 1984.
[27] ——, "Design of error tolerance of a phased array," *Electron. Lett.*, vol. 21, no. 19, pp. 834–836, Sept. 12, 1985.
[28] R. H. Sahmel and R. Manasse, "Spatial statistics of instrument-limited angular measurement errors phased array radars," *IEEE Trans. Antennas Propagat.*, vol. AP-21, pp. 524–532, July 1973.
[29] P. D. Kaplan, "Predicting antenna sidelobe performance," *Microwave J.*, pp. 201–206, Sept. 1986.
[30] R. L. Eisenhart, private communication, 2000.
[31] R. L. Eisenhart and P. K. Park, "Phased array scanning performance simulation," in *IEEE AP-S Int. Symp. Dig.*, 1995, pp. 2002–2005.
[32] R. L. Eisenhart, "Antenna element and array simulation with commercial software," in *Finite Element Software for Microwave Engineering*, T. Itoh, T. Pelosi, and T. Silvester, Eds. New York: Wiley, 1996, ch. 10, pp. 211–235.
[33] L. Stark, "Microwave theory of phased array antennas—A review," *Proc. IEEE*, vol. 62, pp. 1661–1701, Dec. 1974.
[34] G. H. Knittel, A. Hessel, and A. A. Oliner, "Element pattern nulls in phased arrays and their relation to guided waves," *Proc. IEEE*, vol. 56, pp. 1822–1836, Nov. 1968.
[35] R. J. Mailloux, "Surface waves and anomalous wave radiation nulls on phased arrays of TEM waveguides with fences," *IEEE Trans. Antennas Propagat.*, vol. AP-20, pp. 160–166, Mar. 1972.
[36] R. S. Elliott, "Beamwidth and directivity of large scanning arrays," *Microwave J.*, pt. 2, vol. 7, pp. 74–82, Jan. 1964.

Don Parker (S'61–M'63–SM'73–F'82–LF'94) was born in Ogden, UT, on January 14, 1933. He received the B.E.S.E.E. degree from Brigham Young University, Provo, UT, in 1956, the M.S. degree from Harvard University, Cambridge, MA, in 1957, and the Sc.D. degree in electrical engineering from the Massachusetts Institute of Technology, Cambridge, in 1964.

From 1957 to 1961, he was an MIT Lincoln Laboratory Staff Associate. After serving three years as a lieutenant in the U.S. Air Force, he returned to the MIT Lincoln Laboratory in 1964 as a Staff Member. In 1969, he joined the Stanford Research Institute, initially as a Senior Research Engineer and then Director of the Electromagnetic Techniques Laboratory. In 1976, he joined the Hughes Aircraft Company as Manager of the Microwave Department in the Missile Systems Group. He was then Manager of Radar Laboratory and then Assistant Manager of the Radar Laboratories. In 1986, he transferred to the Radar Systems Group within Hughes and became Manager of Active Array Programs in the Engineering Division. In September 2000, he retired from Raytheon Electronic Systems, Dallas, TX, nearly three years after Raytheon purchased Hughes in December 1997.

Dr. Parker is a member of Phi Kappa Phi and Tau Beta Pi. He was secretary in 1972 and a member of the IEEE Microwave Theory and Techniques Society (MTT-S) Administrative Committee (AdCom) from 1973 to 1982. He served as vice president and president of the IEEE MTT-S AdCom in 1978 and 1979, respectively. He was editor-in-chief of the IEEE TRANSACTIONS ON MICROWAVE THEORY AND TECHNIQUES from 1975 to 1978. He was chairman of the Technical Program Committee, for the 1981 IEEE MTT-S International Microwave Symposium (IMS), vice chairman of the 1989 IEEE MTT-S IMS, and chairman of the 1994 IEEE MTT-S IMS. He was the recipient of the 1984 IEEE Fellow Award, the 1985 IEEE Centennial Medal, and the 2000 IEEE Millennium Medal. He was also the recipient of the 1989 Distinguished Service Award of IEEE MTT-S. He was an ABET program evaluator for the IEEE Educational Activities Committee on Accreditation Activities in 1992, 1993, and 1995. From 1992 to 1997, he served as a panel member for electronics and electrical engineering of the National Research Council Board of Assessment of the National Institute of Standards and Technology (NIST) Programs. He was also a member of the Electronics Technology Area Review and Assessment (TARA) Sub-panel of Sensors, Electronics and Battlespace Environments (SEBE) Reliance Panel for the Department of Defense (DoD) Science and Technology Office in 1997, 1998, and 1999.

David C. Zimmermann (M'76) received the B.S. degree in electrical engineering and the M.S. degree in engineering from the University of Texas at Austin, in 1978 and 1979, respectively.

In 1979, he joined the Advanced Technology and Products Division, Defense Systems Group, Texas Instruments Incorporated, where he was initially engaged in hybrid microwave circuit and MMIC design. His early work included design of diode phase shifters, switches, power amplifiers, LNAs, and dual-gate GaAs FET devices for applications through Ku-band. His more recent experience has been in the areas of T/R module and subarray designs for active phased-array development programs. He is currently a Senior Principal Engineer with Raytheon Electronics Systems, Dallas, TX, which acquired the Defense Systems Group, Texas Instruments Incorporated in 1997. He is currently engaged in T/R module development activities for phased-array radar systems.